This paper is published as part of a *Dalton Transactions* themed issue on:

Metal Anticancer Compounds

Guest Editor Peter Sadler

University of Warwick, UK

Published in issue 48, 2009 of *Dalton Transactions*

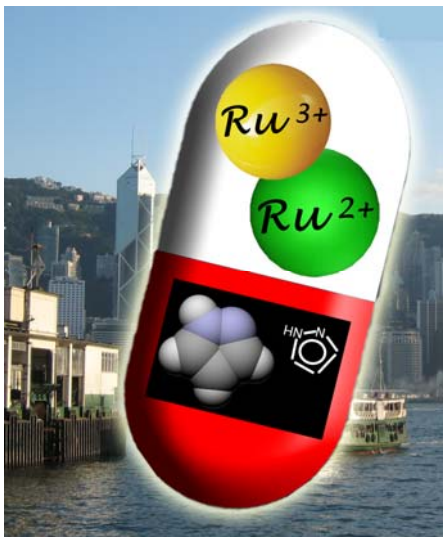

Image reproduced with permission of Chi-Ming Che

Articles published in this issue include:

PERSPECTIVES:

Non-traditional platinum compounds for improved accumulation, oral bioavailability, and tumor targeting
Katherine S. Lovejoy and Stephen J. Lippard, *Dalton Trans.,* 2009, DOI**:** 10.1039/b913896j

Metal complexes as photochemical nitric oxide precursors: Potential applications in the treatment of tumors
Alexis D. Ostrowski and Peter C. Ford, *Dalton Trans.,* 2009, DOI: 10.1039/b912898k

Novel and emerging approaches for the delivery of metallo-drugs
Carlos Sanchez-Cano and Michael J. Hannon, *Dalton Trans.,* 2009, DOI: 10.1039/b912708a

HOT ARTICLE:

Iron(III) complexes of fluorescent hydroxamate ligands: preparation, properties, and cellular processing
Antonia J. Clarke, Natsuho Yamamoto, Paul Jensen and Trevor W. Hambley**,** *Dalton Trans.,* 2009, DOI**:** 10.1039/b914368h

Visit the *Dalton Transactions* website for more cutting-edge inorganic and bioinorganic research
www.rsc.org/dalton

DNA cleavage and antitumour activity of platinum(II) and copper(II) compounds derived from 4-methyl-2-*N*-(2-pyridylmethyl)aminophenol: spectroscopic, electrochemical and biological investigation†‡

Sudeshna Roy,[a] Palanisamy Uma Maheswari,[a] Martin Lutz,[b] Anthony L. Spek,[b] Hans den Dulk,[a] Sharief Barends,[a] Gilles P. van Wezel,[a] František Hartl[c,d] and Jan Reedijk*[a]

Received 12th June 2009, Accepted 4th September 2009
First published as an Advance Article on the web 13th October 2009
DOI: 10.1039/b911542k

The reaction of the redox-active ligand, Hpyramol (4-methyl-2-*N*-(2-pyridylmethyl)aminophenol) with K_2PtCl_4 yields monofunctional square-planar [Pt(pyrimol)Cl], PtL-Cl, which was structurally characterised by single-crystal X-ray diffraction and NMR spectroscopy. This compound unexpectedly cleaves supercoiled double-stranded DNA stoichiometrically and oxidatively, in a non-specific manner without any external reductant added, under physiological conditions. Spectro-electrochemical investigations of PtL-Cl were carried out in comparison with the analogue CuL-Cl as a reference compound. The results support a phenolate oxidation, generating a phenoxyl radical responsible for the ligand-based DNA cleavage property of the title compounds. Time-dependent *in vitro* cytotoxicity assays were performed with both PtL-Cl and CuL-Cl in various cancer cell lines. The compound CuL-Cl overcomes cisplatin-resistance in ovarian carcinoma and mouse leukaemia cell lines, with additional activity in some other cells. The platinum analogue, PtL-Cl also inhibits cell-proliferation selectively. Additionally, cellular-uptake studies performed for both compounds in ovarian carcinoma cell lines showed that significant amounts of Pt and Cu were accumulated in the A2780 and A2780R cancer cells. The conformational and structural changes induced by PtL-Cl and CuL-Cl on calf thymus DNA and ϕX174 supercoiled phage DNA at ambient conditions were followed by electrophoretic mobility assay and circular dichroism spectroscopy. The compounds induce extensive DNA degradation and unwinding, along with formation of a monoadduct at the DNA minor groove. Thus, hybrid effects of metal-centre variation, multiple DNA-binding modes and ligand-based redox activity towards cancer cell-growth inhibition have been demonstrated. Finally, reactions of PtL-Cl with DNA model bases (9-Ethylguanine and 5′-GMP) followed by NMR and MS showed slow binding at Guanine-N7 and for the double stranded self complimentary oligonucleotide $d(GTCGAC)_2$ in the minor groove.

Introduction

The serendipitous discovery of cisplatin and its extensive usage as an antitumour drug have initiated investigations in the medicinal bioinorganic research field towards numerous platinum compounds. Multifactorial resistance (intrinsic or acquired) and severe toxicity limit the prolonged administration of cisplatin, having fuelled search for more potent metallodrugs with less systemic toxicity and internal resistance.[1-3] The other platinum anticancer drugs in clinical practise, or in current clinical trials, include platinum(II)-containing oxaliplatin, carboplatin, picoplatin (JM473), nedaplatin (JM118), or redox-active platinum(IV)-based satraplatin, tetraplatin and ormaplatin. Some of these second or third generation compounds are stable through cell metabolism,[1,3,4] overcome the limitations by less systemic toxicity, have better bio-availability and even display improved antitumour activity.

Genomic DNA is most likely the main cellular target for platinum drugs. Especially for cisplatin it has been demonstrated that the major antitumour activity originates from intrastrand crosslinks and the formation of DNA kinks.[5] Therefore DNA targeting drugs remain in the limelight and compounds acting towards cancer cells selectively over healthy cells, are getting more attention.[6-10] The detailed investigation of cisplatin activation, biotransformation, accumulation, coordinative binding, DNA kinking and unwinding explains much of the antitumour activity of this drug, originating from DNA damage.[11] In recent literature, there are some reports on 'rule-breaker' platinum compounds which are highly active against tumour cells.[12-14] These approaches are focused on the design of compounds that may form adducts

[a]*Leiden Institute of Chemistry, Gorlaeus Laboratories, Leiden University, P.O. Box 9502, 2300 RA, Leiden, The Netherlands*
[b]*Bijvoet Center for Biomolecular Research, Crystal and Structural Chemistry, Utrecht University, Padualaan 8, 3584 CH, Utrecht, The Netherlands*
[c]*Van't Hoff Institute for Molecular Sciences, University of Amsterdam, Nieuwe Achtergracht 166, 1018 WV, Amsterdam, The Netherlands*
[d]*Department of Chemistry, University of Reading, Whiteknights, Reading, UK RG6 6AD*

† Electronic supplementary information (ESI) available: Tables 1 and S2 provide the crystallographic details and bond distances and angles for the compound PtL-Cl. Figs. S1-S12 show the data on crystal packing of PtL-Cl, and details of the characterisation with cellular uptake, DNA binding, ESI-MS and NMR spectroscopic data. CCDC reference number 735958. For ESI and crystallographic data in CIF or other electronic format see DOI: 10.1039/b911542k

‡ Paper dedicated to the memory of the late Lloyd Kelland.

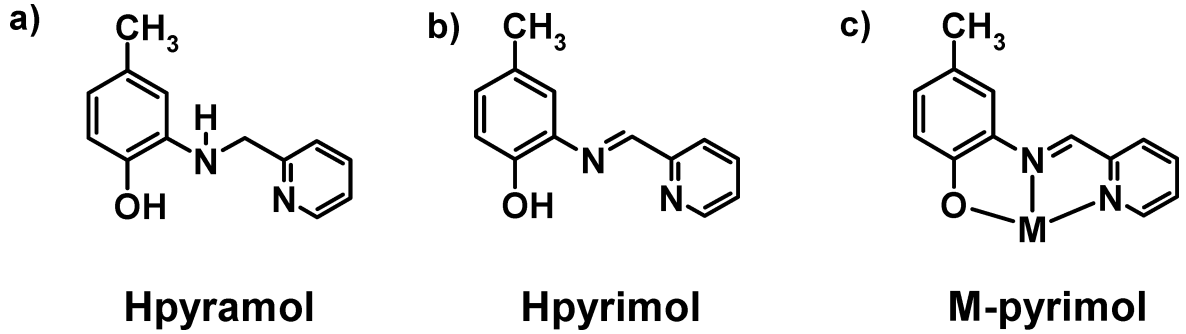

Fig. 1 Schematic structures of (a) Hpyramol, (b) its dehydrogenated form and (c) coordinated to a metal ion.

with DNA, differently than the classical cisplatin. The mode of interaction of newly designed platinum compounds with target biomolecules can be directed either *via* coordinative (interstrand crosslinking), or *via* non-coordinative (intercalation, electrostatic, groove-binding or hydrogen-bonding) interactions.[15,16]

The mono-substituted adduct of cisplatin with guanine has proved to be more genotoxic than the *bis*-guanine adducts.[17] Based on this evidence recently some interesting platinum complexes have been synthesised and investigated which are classified as 'monofunctional' metallodrugs.[18,19] These complexes possess a single labile chloride and therefore after hydrolysis under physiological conditions, they can form only mono-adducts with DNA bases.[20-22] Some of them exhibit interesting antiproliferative activity with increased DNA binding affinity. The monofunctional Pt-ACRAMTU series reported by Bierbach *et al.*[18] for example preferably target the DNA minor groove selectively, due to the presence of a directing intercalator moiety.

Another approach to new antineoplastic metallodrugs could be by making use of the well-known 'chemical nucleases'. This class of compounds cleave DNA in several pathways namely (a) nucleobase oxidation, (b) phosphate ester hydrolysis and (c) deoxyribose sugar oxidation. Such molecular scissors can cleave DNA either by single or double strand breaks. The cellular response from the living organelles against this damage is the activation of multi-faceted repairing mechanisms such as base excision repair, double strand break repair, crosslink repair and nucleotide excision repair. The most efficient chemical nucleases contain transition metal ions, like the redox-active Cu, Fe, or the redox-inactive Zn in their active sites. The classic examples of this type of artificial nucleases used as antitumour drugs are bleomycin and some of its metal-coordinated derivatives along with $[Cu(phen)_2]^+$-based complexes.[23]

From our earlier work, a unique ligand 4-methyl-2-*N*-(2-pyridylmethyl)aminophenol (Hpyramol)[24] forming a compound with $CuCl_2$ (square planar [Cu(pyrimol)Cl], CuL-Cl) was reported to cleave DNA oxidatively and catalytically without any added reductant and to exhibit high to moderate antitumour activity against selected cancer cell lines. The ligand alone is also redox active in solution, but devoid of any DNA cleaving or antineoplastic property towards most cancer cell lines on its own. The protonated ligand form, Hpyrimol (HL), appears to be formed by direct Hpyramol oxidation. Upon metal-ion coordination Hpyramol undergoes oxidative dehydrogenation and concomitant deprotonation to give the anionic ligand 4-methyl-2-*N*-(2-pyridylmethylene)aminophenolate (pyrimol, L^-). A schematic diagram of the ligand, its several forms and coordination patterns with metals is presented in Fig. 1. When coordinated to redox-inactive Zn(II), the Hpyramol ligand cleaves ϕX174 supercoiled phage DNA through a non-diffusible ligand-based radical mechanism.[25,26]

These highly surprising results inspired us to react Hpyramol with platinum(II), which is known to be redox-inactive under physiological conditions; possibly a new potent DNA-targeting anticancer drug might result, that could eventually induce cell death by cleaving the cellular DNA efficiently and irreversibly. Hence, the analogue PtL-Cl was synthesised and structurally characterised by X-ray crystal structure determination, NMR and other experimental techniques as reported below, to correlate the DNA cleavage property and its *in vitro* cytotoxicity towards cancer cell lines. The compounds, PtL-Cl and reference CuL-Cl, were tested for the growth-inhibition of cultured tumour cells. The total drug uptake in the selective cancer cells was also measured. The compound PtL-Cl cleaved ϕX174 phage DNA, as shown by agarose gel electrophoresis, at more than stoichiometric ratio. High resolution PAGE (PolyAcrylamide Gel Electrophoresis) gel experiments were performed to observe any sequence-specific DNA cleavage by PtL-Cl. As DNA is the most expected target here, PtL-Cl was allowed to interact with calf thymus DNA and ϕX174 supercoiled phage DNA. Circular dichroism was used to monitor any conformational changes on its binding. The reactions of PtL-Cl with the model bases 9-ethylguanine and 5′-GMP were followed by ^{1}H and ^{195}Pt NMR to investigate the stability of the mono-adduct with the guanine residue on DNA. The compound PtL-Cl was reacted with self-complementary $d(GTCGAC)_2$ oligonucleotide to detect any solution structural changes upon interaction. A detailed spectro-electrochemical analysis and comparison of the redox behaviour of PtL-Cl with CuL-Cl and Hpyrimol were performed to obtain support for the ligand-based radical-induced oxidative DNA damage caused by PtL-Cl.

Experimental section

Materials

9-Ethylguanine (9-EtG) and Guanosine-5′-monophosphate (5′-GMP) were purchased from Sigma-Aldrich B.V. The ϕX174 supercoiled phage DNA used for DNA cleavage studies was purchased from Invitrogen Life Technology (0.25 μg/μL). Deuterated solvents used for NMR experiments were also purchased from

Sigma-Aldrich. K_2PtCl_4 was used from a generous loan scheme by Johnson-Matthey (Reading, U.K.). The ligand Hpyramol (4-methyl-2-*N*-(2-pyridylmethyl)aminophenol) was synthesised in a single-step reaction as reported in the literature.[24] The solvents used in the syntheses were purchased from Biosolve (AR grade) and used without further purification.

Syntheses

[Pt(pyrimol)Cl], (PtL-Cl). An aerobic ethanolic solution of the precursor ligand, Hpyramol (51.6 mg, 0.24 mmol) was added in the dark drop-wise to an aqueous solution of K_2PtCl_4 (100 mg, 0.24 mmol) and stirred at 50 °C for 24 h. The reaction mixture was filtered while warm and the filtrate was evaporated to 5 mL under reduced pressure. A deep green precipitate was obtained by cooling down this concentrated filtrate at 4 °C overnight. The precipitate was washed with cold ethanol (3 × 2 mL), then with diethyl ether (3 × 5 mL) and dried under suction in the dark. Yield: 65.98 mg (62 %). Elemental analysis for $C_{13}H_{11}N_2OClPt$: C, 35.34; H, 2.50; N, 6.34 (Calcd.), C, 35.25; H, 2.42; N, 6.10 (Expt.). The green precipitate was characterised as Pt(pyrimol)Cl by ^1H, ^{13}C, ^{195}Pt, 2-D COSY and ^1H-^{13}C HETCOR spectroscopy. ^{195}Pt NMR shows a single peak at –2326 ppm (in DMSO-d_6) and –2322 ppm (in DMF), corresponding to a PtN_2OCl coordination environment. Single crystals suitable for X-ray diffraction were grown in the dark from a concentrated DMSO solution in the NMR tube.

[Cu(pyrimol)Cl], (CuL-Cl). The compound CuL-Cl was reproduced by following the method already reported.[26] A deep-red crystalline powder was characterised by elemental analysis, infrared and EPR spectroscopy. A good match with the literature data was observed.

X-ray crystal structure determination of PtL-Cl

Single crystals suitable for X-ray diffraction were obtained directly from an NMR tube which contained a concentrated DMSO-d_6 solution of PtL-Cl and was kept at ambient temperature in the dark. X-ray intensities were measured on a Nonius KappaCCD diffractometer with a rotating anode (graphite monochromator, $\lambda = 0.71073$ Å) at –123 °C. Data were integrated with EvalCCD[27] using an accurate description of the experimental setup for the prediction of the reflection contours. Absorption correction and scaling were performed with the program SADABS.[28] The structure was solved by application of automated Patterson methods (DIRDIF-99[29]). The refinement was performed with SHELXL-97[30] against F^2 of all reflections. Non-hydrogen atoms were refined with anisotropic displacement parameters. All hydrogen atoms were located in difference-Fourier maps and refined with a riding model. Geometry calculations and checking for higher symmetry were performed with the PLATON program.[31] Further details of the molecular structure of PtL-Cl are given in Table 1 and in Supplementary Information (Table S1).†

Table 1 Crystal data and structure refinement for the compound PtL-Cl

formula	$C_{13}H_{11}ClN_2OPt$
formula weight	441.76
crystal colour	dark red
crystal size [mm^3]	$0.21 \times 0.03 \times 0.03$
T [K]	150(2)
λ [Å]	0.71073
crystal system	triclinic
space group	$P\bar{1}$ (no. 2)
a [Å]	7.1447(3)
b [Å]	8.5058(3)
c [Å]	10.2432(3)
α [°]	83.230(2)
β [°]	76.509(1)
γ [°]	87.059(2)
V [Å^3]	600.91(4)
Z	2
D_x [g cm^{-3}]	2.442
μ [mm^{-1}]	11.884
abs. corr.	multi-scan
abs. corr. range	0.36–0.70
$(\sin\theta/\lambda)_{max}$ [Å^{-1}]	0.65
reflections (collected/unique)	9030/2743
parameters/restraints	164/0
$R1/wR2$ [$I>2\sigma(I)$]	0.0246/0.0492
$R1/wR2$ [all refl.]	0.0355/0.0518
$R(int)$	0.0403
S	1.050
$\rho_{min/max}$ [e Å^{-3}]	–1.05/0.94

NMR experiments

The one-dimensional (^1H and ^{13}C) and two-dimensional COSY and HETCOR spectra were recorded on a 600 MHz Bruker DPX600 spectrometer at ambient temperature (24 °C) in DMSO-d_6. The ^{195}Pt spectra were recorded on a 300 MHz Bruker spectrometer with a 5 mm multi-nucleus probe at 24 °C in DMSO-d_6 and non-deuterated DMF solvents. For ^{195}Pt NMR, Na_2PtCl_6 was used as external reference set at $\delta = 0$ ppm.

Biological studies

(a) Cells and culture conditions. The 100 mm culture and micro-well plates were received from NUCLON (Roskilde, Denmark). MTT [3-(4,5-dimethylthiazol-2-yl)2,5-diphenyltetrazoliumbromide] was purchased from Sigma-Aldrich B.V. The human ovarian carcinoma cell lines, cisplatin sensitive (A2780) and cisplatin resistant (A2780R), were generous gifts from Dr. J. M. Perez (Universidad Autonoma de Madrid, Spain). The mouse leukemia cell lines, cisplatin sensitive (L1210/0) and cisplatin resistant (L1210/2), were used for the MTT assay as well. The cells were grown as monolayers in Dulbecco's Modified Eagle's Medium (DMEM) supplemented with 10% fetal calf serum (Gibco, Paisley, Scotland), penicillin (100 units/mL; Dufecha, The Netherlands) and streptomycin (100 μg/mL; Dufecha, The Netherlands). During the culture period the cells grew partly in suspension and partly adhered to the flask wall.

(b) Cytotoxicity assays.

MTT assay. The cell survival was evaluated by a typical MTT colorimetric method[32] *albeit* slightly modified. Cells were plated onto 96-well sterile plates (Corning Co.) in 100 μL of medium at a density of 2×10^3 cells per well and incubated for 48 h at 37 °C in a 7% CO_2 containing incubator. The compound was added at six different concentrations. The final concentrations ranged from 0.4 μM to 90 μM. As the stock solution of PtL-Cl was made in DMF, in order to see the solvent effect, DMF was used as the blank. For comparison the starting ligand (Hpyramol) and cisplatin were tested in the same plate and the stocks in both cases were made in DMF. In addition, for comparison with the reported

value of IC_{50} for cisplatin (in water) the latter was also tested as in a typical aqueous solutions. A freshly prepared MTT solution (5 mg/mL) in PBS buffer was added to each well (50 μL per well) after 48 h of incubation. The plates were then again incubated at 37 °C for 3 h. All the supernatant liquid was removed very carefully without disturbing the blue crystals stuck at the bottom of the plates. The MTT was metabolised by the mitochondrial reduction of the living cancer cells and transformed to a blue formazan product. These crystals were dissolved in 100 μL DMSO per well and were shaken carefully until the crystals were completely dissolved to give a purple solution. The absorbance of each well was determined at 590 nm by using a Model 550 Bio-Rad microplate reader. All the tests were performed in quadruplicate for each cell line. The IC_{50} values were calculated from the curves drawn by plotting % cell survival *versus* compound concentration (in μM) using the program Graphpad Prism, version 3.0, 2000.[16] The IC_{50} value indicates the amount of drug needed for 50% growth inhibition of the cancer cells relative to untreated (drug-free cancer cells).

SRB assay. The cytotoxicities of PtL-Cl, CuL-Cl and the ligand Hpyramol were analysed using the microculture sulforhodamine B (SRB) test,[33] carried out commercially with TEVA-Pharmachemie (Haarlem, The Netherlands). Human tumour cell lines analysed were WIDR, IGROV, M19-MEL, A498 and H226, which belong to the currently used anti-cancer screening panel of the National Cancer Institute, USA[34] with additional two breast cancer cell lines, *i.e.*, MCF-7 (containing estrogen and progesterone receptors) and EVSA-T (lacking both hormone receptors). All cell lines were maintained in a continuous logarithmic culture in the RPMI 1640 medium with the Hepes buffer and phenol red. The medium was supplemented with 10% FCS, penicillin (100 IU/mL) and streptomycin (100 μg/mL). The cells were mildly trypsinised for passage and for the use in the experiments. Trypsinised tumour cells (150 μL, containing 2×10^3 cells/well) were pre-incubated for 48 h at 37 °C in 96-well flat-bottom cell culture plates. The tested compounds were added in a three-fold dilution series up to and including 62.5 μg/mL. After 7 days the cells were fixed with 10% TCA in the PBS buffer and incubated at 4 °C for 1 h. After three times washing with water the cells were stained for 15 min with 0.4% SRB in 1% acetic acid. Subsequently the cells were washed with 1% acetic acid, air-dried and the bound stain dissolved in 150 μL 10 mM Tris-base (unbuffered). The value of A_{540} was assessed using an automated microplate reader (Labsystems Multiskan MS). Data were used for concentration-response curves and ID_{50} values using Deltasoft 3 software (Biometallics Inc., Princeton, NJ, USA).[16] Subsequent conversion of units provided the IC_{50} values for all samples tested.

(c) Cellular uptake experiments. Cells of the A2780 and A2780R cell lines were plated in sterile 6-well plates in 5 mL of Dulbecco's Modified Eagle's Medium (DMEM) at a density of 1×10^5 cells per well and incubated for 48 h. The cisplatin, CuL-Cl and PtL-Cl were added to the plates at the ultimate concentration of 200 nM, and incubated for 2, 6 and 24 h. Afterwards the cells were washed twice with 5 mL PBS per well and triton (lysis buffer) was added (350 μL per well) to lyse the cells. After transferring the pellet to Eppendorf tubes, 10% SDS (100 μL per well) and Proteinase K (20 μg/mL and 1 mL per well) were added. Then the viscous pellets were incubated at 55 °C for 30 min and 1.5 mL 20% HNO_3 was added. After shaking for 45 min the samples were measured by Varian Vista-MPX charge-coupled simultaneous ICP-OES (Inductively Coupled Plasma Optical Emission Spectroscopy) to estimate of % Pt and % Cu taken up by the cancer cells. To compare the accumulation of Pt-moieties inside the cisplatin sensitive, A2780 cells, time-dependent uptake studies were also performed for PtL-Cl at 2 h intervals for up to 24 h. The active concentration of PtL-Cl used for the time-dependent measurement was 50 μM.

(d) DNA cleavage studies. ϕX174 supercoiled phage DNA was purchased from Invitrogen Life Technologies and stored at –20 °C. A typical reaction mixture, containing supercoiled plasmid DNA and PtL-Cl in a 10 mM phosphate buffer at pH 7.2, was incubated at 37 °C for 2 h (with or without additives, or without any external reductant). After the incubation period, the reaction was quenched by keeping the samples at –20 °C, followed by the addition of loading buffer (bromophenol blue, xylene cyanol, and 25% ficoll). This was then loaded on a 0.8% agarose gel containing ethidium bromide (2.54 μM in the gel as well as in the buffer). The gels were run at a constant voltage of 80 V for 60-90 min in the TBE buffer containing ethidium bromide. After washing with distilled water, the gels were visualised under a UV transilluminator and the bands were documented and quantified using a BioRad Gel Doc 1000 apparatus interfaced with a computer.

(e) High resolution denaturing gel electrophoresis.

Preparation of oligonucleotides and PAGE. For the high resolution analysis of the DNA cleavage process, a double-stranded oligonucleotide was used. The synthetic procedure to prepare this type of oligonucleotides has a coupling efficiency of 97-99%. Therefore, in each step, a short side product is formed, whose intensity on the electrophoresis gel is associated with the coupling efficiency (a 99% efficiency implies that 1% side product is present, 97% gives 3% side product and so on). Consequently, the electrophoresis reveals a ladder-like pattern, with a weak band at each nt (nucleotide) position. This is ideally suited for the detailed analysis of the cleavage mechanism. A 54 nt oligonucleotide FNA1 (DNA sequence 5′-GATCCTGGTGGAGCTAAGCGGGATCGAACC-GCT-GACCTCTTGCTTGCATAGCAA-3′) was radiolabelled with [γ-^{32}P]ATP (MP Biomedicals) using T4 polynucleotide kinase (Fermentas) as indicated by the supplier, and purified over S200 spin columns (GE healthcare), effectively removing all products up to 15 nt.[35] Duplex DNA was obtained by annealing the 10 μM [^{32}P]-labelled FNA1 with an equimolar amount of oligonucleotide FNA2 (5′-AGCGCTTGCTATGCAAGCAAGAGGTCAGCGGTTCG-ATCCCGCTTAGCTCCACCA-3′) in 250 mM NaCl solution at 70 °C for 2 min, followed by slow cooling to ambient temperature. On either side, the probe has 5 nucleotides of a single-stranded region at the 5′ end (underlined in the oligonucleotides). For copper-induced cleavage experiments, the FNA1/2 duplex DNA was incubated at a concentration of 100 μM bp with 20 μM of compound, CuL-Cl at 37 °C. At indicated time intervals (0-60 min), samples were taken and quenched with an equal volume of stop solution (90% [v/v] formamide and 50 mM H_4edta) at –20 °C.[26] DNA was incubated at a concentration of 100 μM bp with 50 μM and 200 μM of platinum compound, PtL-Cl at 37 °C at indicated time intervals (0-150 min). Samples were separated

by high resolution denaturing PAGE (15%) and visualised by phosphor imaging (Bio-Rad).

Enzymatic religation. pUC19 plasmid DNA was treated with PtL-Cl, CuL-Cl, or with the restriction enzyme *BamH1*, without any reductant, at 37 °C and at pH 7.2. DNA samples were purified over QIAquick PCR purification columns (Qiagen) and used for religation experiments. The ligation reaction was performed in a 20 μL volume using 50 ng of the digested DNA products with 2 units of T4 DNA ligase (Fermentas) for 16 h at 16 °C.

(f) Circular dichroism. Circular dichroism spectra were recorded at 37 °C using a Jasco J-815 spectropolarimeter equipped with a Jasco PTC-423 S Peltier temperature controller. The scanning rate was 100 nm/min with a response time 1 s. Spectra were recorded at standard sensitivity (100 mdeg) with a data-pitch of 0.5 nm in continuous mode. The scanning range was 320-220 nm and all the spectra were average of four consequent accumulations. The cuvettes used were 2 mm Quartz Suprasil precision cells (Hellma). The baseline was corrected using 10 mM phosphate buffer as a reference. Volume of sample in the cuvettes was kept constant at 700 μL.

A typical sample containing DNA (Calf thymus DNA or supercoiled ϕX174 phage DNA) and metal compounds (PtL-Cl or CuL-Cl) in phosphate buffer was incubated at 37 °C and the CD spectra were collected at the given time intervals. As references, cisplatin and the free ligand, Hpyramol were also interacted with DNA under similar conditions as followed for PtL-Cl or CuL-Cl.

(g) Electrochemical studies. Cyclic voltammetry of 1×10^{-3} M PtL-Cl in a single-compartment cell was carried out with an Autolab PGstat10 potentiostat (Eco Chemie) controlled by GPES4 software, or with an EG&G PAR Model 283 potentiostat operated with the PAR Power CV® software. The DMF solutions contained 10^{-1} M Bu_4NPF_6 as the supporting electrolyte. The three-electrode system consisted of a carefully polished Pt disk working electrode, a Pt auxiliary electrode, and an Ag/AgCl reference electrode. The voltammetric response of the standard ferrocene/ferrocenium (Fc/Fc^+) couple was found in this system at +0.43 V *vs* Ag/AgCl. The air-tight UV-Vis spectroelectrochemical cell employed for the *in situ* oxidation of 2×10^{-3} M of PtL-Cl and the ligands Hpyramol and Hpyrimol at room temperature, has been described in detail elsewhere.[36] The electrode potential was controlled during the in situ electrolyses by a PA4 potentiostat (EKOM, Polná, Czech Republic). UV-Vis spectra were recorded with a HP 8453 diode array spectrophotometer.

(h) Reactions with model bases.

NMR experiments. The compound PtL-Cl (4 mM) was allowed to react with 9-ethylguanine and 5′-GMP at different stoichiometric ratios. The solvents used were DMSO-d_6 (for 9-Ethyl guanine) and DMSO-d_6/D_2O mixture (for 5′-GMP) studies in an NMR tube. The reactants were mixed prior to the measurements, where the time interval between the mixing and recording of the first spectrum was maximum 15 min The experimental temperature was maintained at 37 °C (for pseudo-physiological conditions) for overnight series ^{1}H NMR experiments. After 14 h the samples were kept in a water bath for maximum 30 days at 37 °C and spectra were recorded at different time-intervals. ^{195}Pt NMR spectra were recorded after 24 and 48 h to observe the changes in the Pt coordination sphere.

ESI-MS measurements. All the spectra were recorded on a Finnigan AQA instrument equipped with electrospray interface (ESI). The reactions between PtL-Cl and model bases (9-ethylguanine and 5′-GMP) were followed by ESI-MS at time intervals of max 15 min up to 3 h, and also after 24 h. The solvents used were DMSO and a DMSO/H_2O 1:1 mixture (v/v) for the two model bases, respectively. The samples from the NMR tubes were also directly used to identify reaction products.

(i) NMR Solution studies with d(GTCGAC)$_2$. ^{1}H NMR spectra were recorded on a Bruker 600 MHz spectrometer. The temperature was varied from 7 to 47 °C to determine the fast exchange kinetics. Afterwards the 2-D NOESY spectra were recorded by the method[37] of States *et al.* using 2048 data points in t_2 for 256 t_1 values with a pulse repetition delay of 2 s at 17 °C or 27 °C. DQF-COSY experiments were also accumulated using 2048 data points in t_2 for 256 t_1 values with a pulse repetition delay of 2 s. Spectra recorded in 90% H_2O and 10% D_2O were collected using the WATER GATE solvent suppression technique of Piotto *et al.*[38] ^{1}H chemical shifts are relative to (tetramethylsilyl)propionic acid (TSP) as internal standard. Typical samples contained 1 mM d(GTCGAC)$_2$ duplex, 1 or 2 mM PtL-Cl, 20 mM NaCl in D_2O, and 10 mM phosphate buffer (pH = 7) in 0.5 mL of H_2O.

Results and discussion

Synthesis

The chemical synthesis of PtL-Cl is straightforward and successfully completed in a single step. K_2PtCl_4 and the ligand Hpyramol are reacted in equimolar ratio to yield the compound PtL-Cl as a crystalline green powder. The spectroscopic and elemental analyses prove the formation as PtL-Cl. The ^{195}Pt NMR shows a single peak (at –2326 ppm), which is in the region common for PtN_3O and PtN_3Cl coordination environments.[39,40] No evidence is observed of any fold-back signal, so the single peak can be attributed to a PtN_2OCl environment. No attempts were undertaken to study the stepwise dehydrogenation of Hpyramol in the presence of K_2PtCl_4 under anaerobic conditions or otherwise, as the reactions had always been performed under aerobic conditions. The ESI-MS of PtL-Cl in DMSO solution shows a major peak at $m/z = 484.32$, which corresponds to the cation $[Pt(pyrimol)(dmso)]^+$ formed after the solvolysis of relatively labile chloride ligand by DMSO. The C,H,N elemental analysis also fits with the elemental percentage calculated for PtL-Cl.

Crystal structure description

Needle shaped single crystals of PtL-Cl were obtained by slow evaporation of a concentrated DMSO-d_6 solution in an NMR tube at ambient temperature under exclusion of day light. The crystal structure shows the starting ligand Hpyramol to dehydrogenate and coordinate to Pt(II) through the N_2O-binding motif, which results in an almost square-planar geometry with *cis* angles between 81.74(15)° and 99.14(11)° (Fig. 2). The molecular structure is quite similar to the reported CuL-Cl,[26] but the packing in the crystal lattice is completely different, apparently due to the co-crystallised H_2O in CuL-Cl. The planar PtL-Cl molecules are stacked on top of each other in an anti-parallel fashion in the direction of the crystallographic *a*-axis (Fig. S1†) with

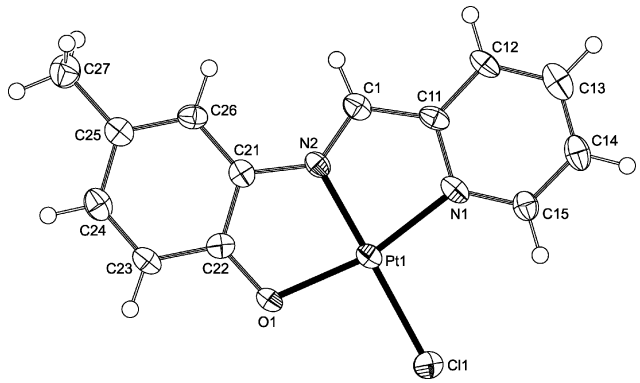

Fig. 2 Displacement ellipsoid plot of PtL-Cl in the crystal (50% probability level).

intermolecular Pt···Pt distances of 5.0418(3) and 4.7540(3) Å. The corresponding interplanar distances are 3.43 and 3.31 Å, respectively. Besides this molecular stacking no other strong intermolecular interactions could be detected. This observation is understandable, as no strong hydrogen bond donors are present. Consequently the long dimension of the needle shaped crystals corresponds to the crystallographic *a*-axis. In CuL-Cl there is also anti-parallel molecular stacking in the *a*-direction, with Cu···Cu distances of 5.1647(3) and 6.1325(3) Å and interplanar distances of both 3.34 Å; however, the stacks are linked with each other by intermolecular hydrogen bonds involving the co-crystallised H_2O molecules. More relevant crystallographic data for PtL-Cl are available in the Supporting Information (Tables 1 and S1†).

Cytotoxicity assays

MTT assay. The *in vitro* cytotoxicity tests were performed for human ovarian carcinoma and mouse leukemia cancer cell lines (See Experimental for details). The IC_{50} values (in μM) are summarised in Table 2 with their respective standard deviations. In ovarian carcinoma cell line (both cisplatin sensitive and resistant) the IC_{50} values for PtL-Cl are very high (22.4 and 43.6 μM, respectively), which indicates its low activity when compared to leukemia cell line (8.1 and 27.5 μM, respectively). The IC_{50} values in cisplatin resistant cell lines are higher than in cisplatin sensitive cell lines, which is generally observed. In leukemia cell lines PtL-Cl overcomes cisplatin resistance to some extent as evident from the RF value of 3.4. Therefore, the compound PtL-Cl is active towards leukemia cell line and moderately active towards ovarian carcinoma cell lines. CuL-Cl shows very high antiproliferative properties in these four cell lines, as in all cases the IC_{50} values are similar or even lower than the IC_{50} values for cisplatin itself and this compound overcomes cross-resistance to cisplatin in both types of cancer cell lines. On the other hand, free Hpyramol is active in ovarian carcinoma cell lines, but in leukemia cell lines it exhibits almost no activity. It is therefore evident that the cytotoxicity profile has changed significantly after coordination with Pt(II) or Cu(II). For comparison cisplatin was also tested after dissolution in DMF, similarly as PtL-Cl and free ligand. It is evident from the table that the IC_{50} values calculated for cisplatin (in DMF) are quite different than the IC_{50} values for cisplatin in aqueous solution. This observation indicated that, although DMF is known as a weakly coordinating solvent, in some cases it can also act like a coordination solvent (replacing coordinated chloride) and the solvated species can result in a different biodistribution.

The effect of different times of incubation on the activity towards cell lines has also been investigated. The cytotoxic activity of PtL-Cl was found to be reduced with longer incubation time. The IC_{50} values are increased by 2-fold (A2780), 3-fold (A2780R), 18-fold [L1210(0)] and 4-fold [L1210(2)], respectively. When the incubation time is shorter, CuL-Cl exhibits a high activity, *i.e.* as high as cisplatin, whereas longer incubation times repress the activity. The results are shown in Table 2 for incubation times 48 h and 120 h. The loss of activity in resistant cell lines, A2780R and L1210(2) is more significant than in the case of the cisplatin sensitive, A2780 and L1210(0) cell lines. The prolonged incubation time reduced the activity of CuL-Cl up to eighteen to twenty times in cell lines tested. The differences can be explained by either by increased efflux, or by increased cellular assimilation of the biologically relevant metal ion, Cu(II), in CuL-Cl. In case of cisplatin and PtL-Cl, the results can be explained also by enhanced efflux and slower cellular uptake.

SRB assay. Seven human tumour cell lines with different origin were used to test the activity of PtL-Cl and CuL-Cl. For cisplatin and CuL-Cl stock solutions were made in MilliQ water, while for PtL-Cl, DMSO is used to make the stock solution. The results are summarised in Table 3. The activity profile clearly shows a dependence on the time of incubation. For all cell lines, the activity of cisplatin was found higher with prolonged incubation.

The activity of cisplatin after 120 h of incubation was six to twelve times higher than after 48 h of incubation. This difference

Table 2 IC_{50} values in μM of samples against human ovarian carcinoma and mouse leukaemia cancer cell lines (cisplatin sensitive and resistant) after 48 h and 120 h of incubation

Samples	Time (h)	A2780	A2780R	RF[a]	L1210(0)	L1210(2)	RF
Cisplatin (water)	48	2.9 ± 0.2	13.1 ± 0.2	4.5	4.0 ± 0.3	24.2 ± 0.2	6.1
Cisplatin (DMF)		8.6 ± 0.4	17.2 ± 0.3	2.0	5.6 ± 0.2	14.6 ± 0.7	2.6
Hpyramol (DMF)		15.0 ± 0.3	13.8 ± 0.3	0.9	>>50	>50	—
PtL-Cl (DMF)		22.4 ± 0.4	43.6 ± 0.5	1.9	8.1 ± 0.3	27.5 ± 0.3	3.4
CuL-Cl (water)		3.4 ± 0.2	8.3 ± 0.6	2.4	3.6 ± 0.2	10.3 ± 0.3	2.9
Cisplatin (water)	120	1.1 ± 0.2	21.9 ± 0.7	19.9	3.1 ± 0.6	39.7 ± 0.4	12.8
PtL-Cl (DMF)		38.8 ± 0.2	120.9 ± 0.8	3.1	42.2 ± 0.4	121.6 ± 0.8	2.9
CuL-Cl (water)		63.9 ± 0.5	158.8 ± 0.7	2.5	62.8 ± 0.4	153.8 ± 0.6	2.4

[a] The Resistance Factor (RF) is defined as the relative ratio of IC_{50} values in resistant and sensitive variety of similar cell lines, *e.g.*, A2780R/A2780 or L1210(2)/L1210(0), respectively. IC_{50} value is defined as the amount of a compound needed to inhibit 50% of cell growth. The deviations are incorporated with the values.

Table 3 IC_{50} values in μM of samples against seven human tumour cell lines after 48 h and 120 h of incubation

Samples	Time (h)	A498	EVSA-T	H226	IGROV	M19-MEL	MCF-7	WIDR
Cisplatin	48	8.2	17.2	10.4	3.0	9.7	16.3	21.1
PtL-Cl		51.5	26.2	69.5	24.8	59.3	31.5	50.9
CuL-Cl		33.4	1.3	29.4	18.6	2.2	21.4	36.2
Cisplatin	120	6.2	2.5	2.1	0.74	2.3	2.7	1.8
PtL-Cl		8.8	38.4	56.6	45.2	54.4	27.4	62.7
CuL-Cl		4.3	10.6	11.5	17.2	1.5	10.6	29.9

can be explained by higher accumulation over a longer time-period and reduced efflux. In the case of PtL-Cl, there is no smooth trend of change. The activity of PtL-Cl, in the A498 cell line, was increased by six folds after 120 h (IC_{50} values range 51.5 μM to 8.8 μM) incubation. In the H226 and MCF-7 cell lines the activity of PtL-Cl was found to be enhanced as well. For other cell lines no prominent effect of time-period of incubation was noticed. The significant change in activity was also observed in the case of CuL-Cl. In the A498, H226 and MCF-7 cell lines the activity of CuL-Cl was found increased by seven, two and two times, respectively. In the other three cell lines, *i.e.* IGROV, M19-MEL and WIDR, the activity of CuL-Cl was also found increased, but to a smaller extent. A completely contrasting behaviour was observed in the EVSA-T cell line, where the activity of CuL-Cl is repressed by almost eight times upon longer incubation times. Apparently the changes in activity profile are strongly dependent on the time of incubation and consequently on uptake and efflux, deactivation and interaction with cellular targets.

The variability of the *in vitro* cytotoxicity test depends on the cell line used and the serum applied. With the same batch of cell lines and the same batch of serum the interexperimental CV (coefficient of variation) is 1-11% depending on the cell line, and the intraexperimental CV is 2-4%. These values may be higher when using other batches of cell lines and/or serum.

Uptake of PtL-Cl and CuL-Cl in ovarian carcinoma cells

In order to explain the huge difference in the cytotoxicities (PtL-Cl and CuL-Cl), uptake studies have been performed in A2780 and A2780R cell lines. The amount of Pt or Cu which were taken up by both cisplatin sensitive and resistant ovarian carcinoma is shown in Figs. 3a and 3b, respectively. In the A2780 cell line the platinum compounds, both cisplatin and PtL-Cl, were accumulated increasingly inside the cells with gradual increase in incubation time, whereas the Cu-compound, CuL-Cl, is accumulated at its highest concentration after 24 h incubation. The amount of Pt accumulated inside the A2780 cells is similar when compared to cisplatin, which is not at the same line with its lower cytotoxicity. The Cu-accumulation does not follow any smooth trend as after 6 h there is some excretion and after 24 h a significant amount of Cu can be detected. This extent of accumulation can easily explain the high activity of compound CuL-Cl in ovarian carcinoma cell lines.

In resistant cell lines the same trend was followed by the platinum compounds, but maximum accumulation of Cu was found to be achieved after 24 h, after some initial excretion at 6 h. As the resistant cell lines are obtained after multiple exposures of cell lines to cisplatin over a certain time period, the uptake of Pt-compounds is expected to be lower than for the sensitive counterpart. The data observed for cisplatin are in agreement with the expected value, even though PtL-Cl exhibits a different behaviour. Although a significant amount of platinum derived from the compound PtL-Cl was detected and shown to be accumulated in a higher amount compared to cisplatin in the cell, the low cytotoxicity cannot be directly related. The deactivation by cellular platinophiles can be the most plausible explanation. On the contrary, Cu is more abundant in the physiological environment; the cellular uptake for Cu-compound would be

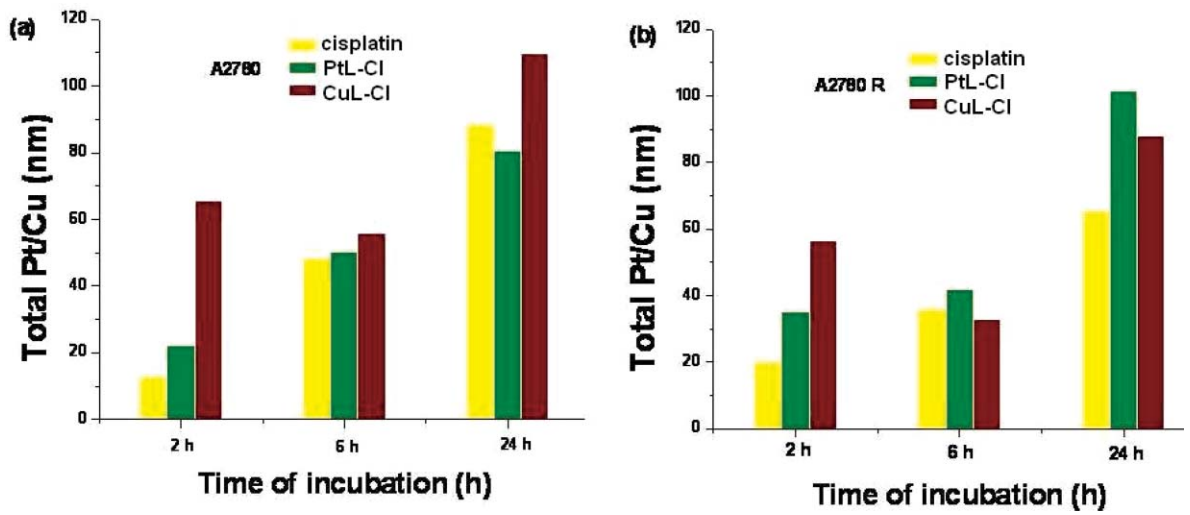

Fig. 3 Amount of Pt/Cu accumulated inside (a) A2780 and (b) A2780R cell-lines at different incubation times from cisplatin, PtL-Cl and CuL-Cl.

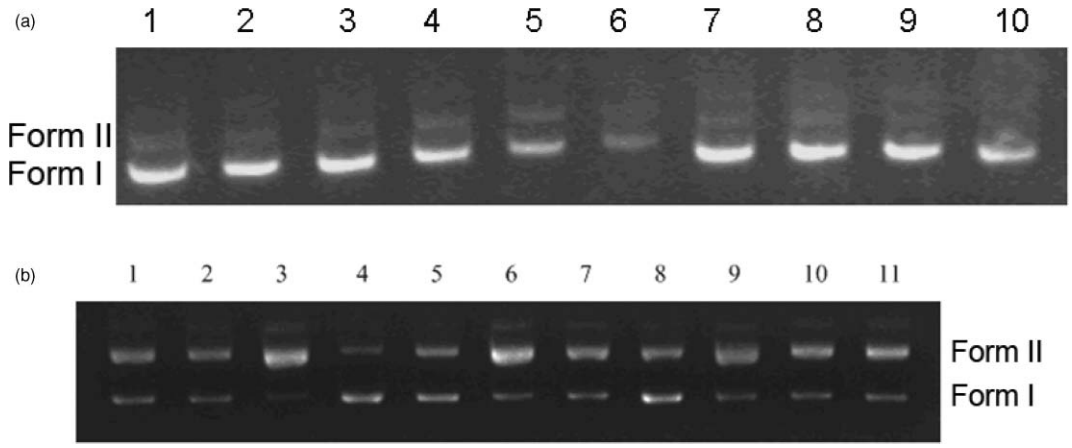

Fig. 4 **a.** Agarose gel electrophoresis of ϕX174 supercoiled phage DNA incubated with PtL-Cl at 37 °C, in the phosphate buffer at pH = 7.2. **Lane 1**, DNA blank (20 μM in base pairs), **lane 2**, 20 μM DNA + 10 μM of PtL-Cl, **lane 3**, 20 μM DNA + 20 μM of PtL-Cl, **lane 4**, 20 μM DNA + 50 μM of PtL-Cl, **lane 5**, 20 μM DNA + 100 μM of PtL-Cl, **lane 6**, 20 μM DNA + 200 μM of PtL-Cl, **lane 7**, 20 μM DNA + 10 μM of PtL-Cl + 20 μM ascorbic acid, **lane 8**, 20 μM DNA + 20 μM ascorbic acid, **lane 9**, 20 μM DNA + 10 μM of PtL-Cl +20 μM TEMPO, **lane 10**, 20 μM DNA + 20 μM TEMPO. **b.** Agarose gel electrophoresis of the oxidative cleavage reaction of ϕX174 supercoiled phage DNA (20 μM in base pairs) with PtL-Cl (100 μM) without reductant after an incubation time of 2 h at 37 °C in the phosphate buffer at pH = 7.2 (**lanes 10** and **11**), in the presence of the following species: for **lane 1**, 200 μM NaN_3; **lane 2**, DMSO; **lane 3**, 0.5 U of superoxide dismutase; **lane 4**, 100 μM distamycin; **lane 5**, ethanol; **lane 6**, D_2O; **lane 7**, 350 mM NaCl; **lane 8**, reaction performed under an argon atmosphere; **lane 9**, reaction with exclusion of light.

expected to be faster than for the toxic metal compounds, cisplatin and PtL-Cl. The uptake or accumulation pathway of the CuL-Cl is most likely to be different from that of platinum compounds, as relatively higher amounts of Cu can be detected.

In order to quantify the amount of platinum accumulated inside the A2780 cells with a certain time interval (2 h), a separate experiment was performed with 50 μM of PtL-Cl. The maximum accumulation observed after 18 h of incubation but the time-scale of cancer cell-cycle is around 24 h. The changes in the amount of platinum accumulated inside the cells do not follow a specific trend, which may be interesting to be studied in more details. In Fig. S2† the concentration of platinum inside the cell *versus* incubation time has been plotted to draw a correlation of the uptake-accumulation and cytotoxicity *in vitro* for compound PtL-Cl. After the initial higher accumulation of Pt in cells, the efflux process becomes most probably activated and the amount of total platinum inside the cells gradually decreases. After 10 h of incubation, the uptake and accumulation is starting to reach the highest concentration at 18 h. After that time PtL-Cl appears to be excreted from the cells and the accumulation of platinum after 24 h is relatively higher than the initial accumulation. This study, however, do not follow the same trend as described above (with 200 nmol/L active concentration of PtL-Cl). Therefore, after a complete cell-cycle a significant accumulation of platinum has taken place, although it cannot be correlated with the *in vitro* cytotoxicity data. This behaviour can be explained by platinum removal or deactivation with platinophiles inside the cells.

DNA cleavage studies

Agarose gel electrophoresis. The DNA cleaving ability of PtL-Cl was investigated on reaction with ϕX174 supercoiled phage DNA and relative mobility of the products on agarose gel. PtL-Cl (20-200 μM) was incubated with DNA (20 μM in base pairs) for 2 h at 37 °C in phosphate buffer (pH = 7.2), with or without additives and reductant. On binding of an increasing amount of PtL-Cl, the DNA shows significant retardation in mobility during electrophoresis (Fig. 4a; illustrated by the slower migration of the bands), most likely caused by the increased amount of adduct formation between the DNA and the metal compound. The smear above the DNA is most likely indicative of the disintegration of the complex between PtL-Cl and DNA during electrophoresis. Interestingly, little difference is observed in terms of DNA cleavage between 0-20 μmol/L PtL-Cl, suggesting that DNA cleavage only occurs after binding of multiple molecules of metal compounds. This is supported by the observation that at concentrations of 50 μM and higher extensive cleavage is seen, with complete obliteration of the DNA at 200 μM, and that hardly any nicked DNA (Form II, resulting from a single cleavage event) and no linear DNA (Form III, double-strand cleavage) is observed. During oxidative cleavage a more canonical cleavage pattern was observed, with discrete bands and the expected formation of Form II (Fig. 4b). This observation illustrates that under these conditions nicking occurs on the intact (full-length) ϕX174 DNA, while the absence of linear DNA highlights the lack of double-strand cleavage. The added reductant (lane 7, 100 μM ascorbic acid) or the radical scavenger (lane 9, 20 μM TEMPO) do not affect the cleavage activity of PtL-Cl. With 200 μM PtL-Cl, the DNA is completely digested. Thus, PtL-Cl behaves differently from CuL-Cl, as the latter compound cleaves DNA oxidatively and catalytically.[26] With this concentration-dependent experiment, however, "single-strand nicking" and "non-catalytic (stoichiometric) cleavage" processes are difficult to discriminate with certainty.

The DNA cleavage reactions carried out with PtL-Cl are not inhibited by the presence of various radical scavengers, that is, NaN_3, superoxide dismutase, DMSO, ethanol or D_2O (Fig. 4b). The use of distamycin highly inhibits the DNA cleavage and an excess of NaCl does not inhibit the cleavage of DNA, and Form II is still detected if the digestion is performed under argon,

or reaction with exclusion of light. These results point to the binding of PtL-Cl preferably in the minor groove as competed by distamycin, and to non-diffusible radical pathways of DNA cleavage.

High-resolution analysis of the cleavage process. To study the non-oxidative cleavage phenomenon in more detail, high resolution DNA electrophoresis studies were performed, which allowed for the separation of DNA fragments with single nucleotide resolution (see below). This experiment was performed using a 5′ radiolabelled double-stranded oligonucleotide, which was known to produce a ladder of bands inherent to the fact that each coupling step occurs with a 98-99% efficiency. The samples were then run on a 15% denaturing gel, to allow identification of DNA fragments at single nucleotide resolution. Excitingly, while the control lane clearly showed individual bands, on progressive degradation these simply became fainter (more prominent for 200 μM DNA and 90 min incubation), eventually producing a continuous 'smear' (Fig. 5). This smearing is most likely the result of the cleavage process and is not due to excessive background, as highlighted by the intensity of the smear below the lowest nucleotide band (15 nucleotide (nt), see bottom part of Fig. 5). PtL-Cl, therefore attacks the DNA at multiple sites without any specificity like the CuL-Cl. In fact CuL-Cl degrades the DNA in a very non-specific manner, perhaps attacking the base and/or the sugar in multiple positions (Fig. 5).

The mode of DNA cleavage activity (oxidative or hydrolytic) towards pUC19 DNA by compound PtL-Cl and CuL-Cl was investigated by transformation to *E. coli* competent cells. DNA was linearised with a restriction enzyme (*Bam*HI) (as a control), or incubated with one of the compounds PtL-Cl or CuL-Cl. Next, DNA was purified to remove the excess of metal compounds, dissolved in water, and measured by the nano-drop spectrophotometer to determine its concentration exactly. The digestion mixture (5 ng) was then religated by T4 DNA ligase and transformed to fresh competent cells of *E. coli*, to determine the number of colony forming units (CFU). Comparison of the transformation efficiencies of uncleaved pUC19 DNA with the control experiment (*Bam*HI digested and religated using DNA T4 ligase) showed that the ligation efficiency was close to 95%. Each experiment was performed in triplicate, giving highly reproducible results.

In Fig. 6 DNA digested with the restriction enzyme BamHI is set to 100% religation efficiency, since restriction enzymes generate intact 3′- and 5′- DNA ends that form a perfect template for ligation. For the copper compound, the bar is somewhat lower, indicating that the religation efficiency is reduced by just over an order of magnitude, while the very low bar for the Pt complex indicates approximately 1000-fold lower religation efficiency compared to the restriction enzyme. The formation of DNA ends that cannot be religated strongly suggests oxidative cleavage, as this process will result in template ends that are not recognized by the DNA ligase. The high religation efficiency observed with DNA digested by CuL-Cl, shows that the oxidative DNA cleavage efficiency of the CuL-Cl compound is lower than that of PtL-Cl for the same amount of pUC19 DNA; however it is still significant. The fact that Pt(II) is unlikely to change valence state in this process, points towards a phenoxyl-based process.

Circular dichroism

The DNA conformational changes induced by PtL-Cl, CuL-Cl and Hpyramol were investigated by CD spectroscopy. Typical

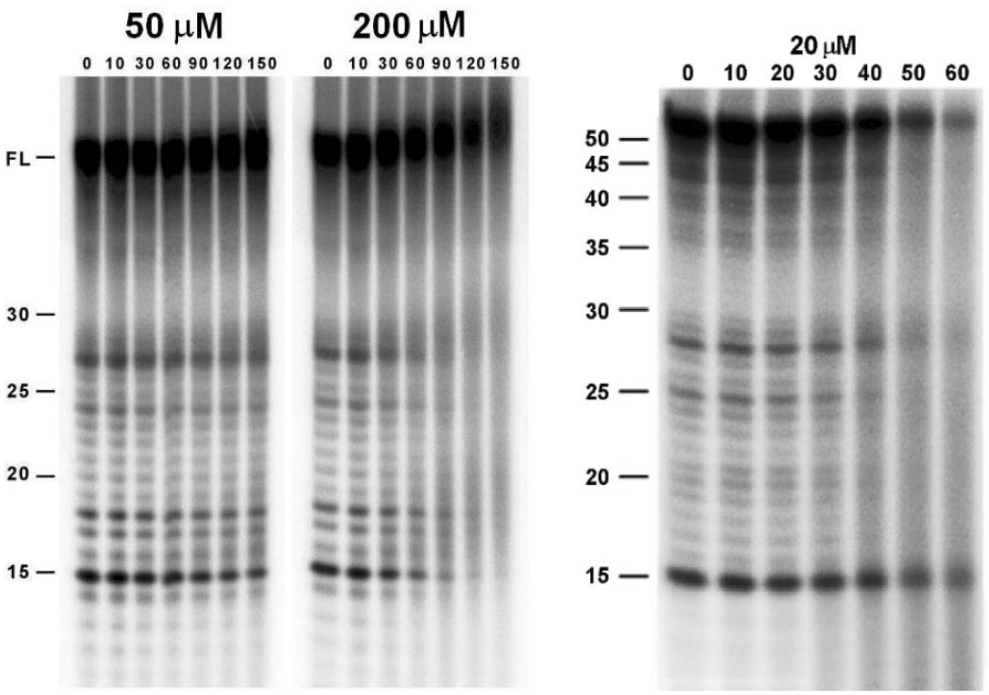

Fig. 5 High-resolution analysis of the cleavage process induced by the compounds PtL-Cl and CuL-Cl. A 54 base pair double-stranded DNA fragment was incubated with PtL-Cl for 0-150 min (left) and with CuL-Cl for 0-60 min (right). DNA size marker in nucleotides (nt) is shown on the left side of the figure. Time (min) is indicated above the lanes. The probe was uniquely radiolabeled at the 5′ end of the top strand. Smearing demonstrates multiple cleavages of nucleotides.

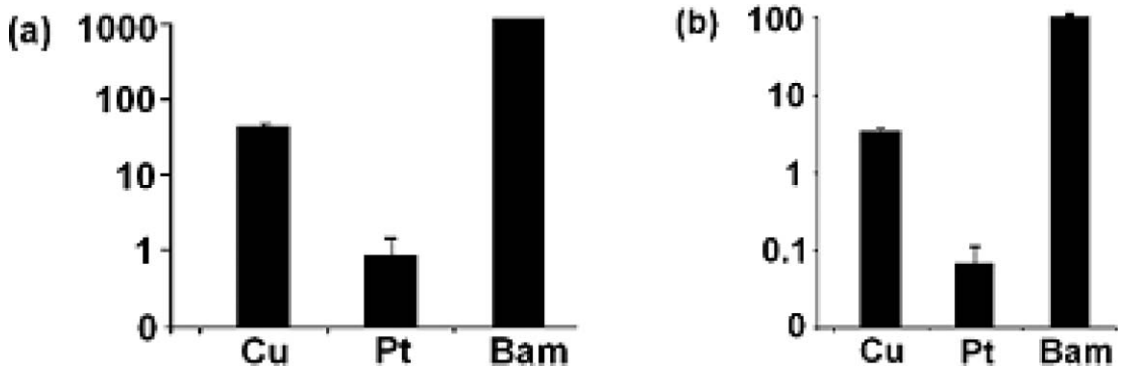

Fig. 6 Relative efficiency of cleavage activity of PtL-Cl and CuL-Cl on pUC19 DNA as (a) CFU per ng DNA and (b) relative CFU. **Bam**: DNA digested with restriction enzyme *Bam*HI; **Cu**: DNA cleaved with CuL-Cl and **Pt**: DNA cleaved with PtL-Cl. In all experiments the DNA was religated with T4 DNA ligase and then transformed to *E. coli* cells. CFU, colony forming units after transformation of *E. coli* cells with the DNA samples. Note that Cu-cleaved DNA was restored much more efficiently by religation than Pt-cleaved DNA.

samples contained calf thymus DNA (CT DNA, 100 μM per base) in the presence or absence of a metal compound (1 mM) in 10 mM phosphate buffer (pH = 7.2). The ionic strength was kept constant at 50 mM. Therefore, the R value remained constant at 0.1 for all investigated compounds. The metal compounds do not exhibit any CD in the chosen region of scan. The samples were incubated at physiological temperature (37 °C) and the CD spectra were recorded at certain time intervals (10 min intervals up to 60 min and then 1 h intervals up to 12 h of incubation time). Cisplatin was used as a reference under identical experimental conditions. The changes observed in the native right-handed B-form DNA on interaction with the compounds are shown in Fig. 7(a-d). The panels 7a and 7b show the changes in the CD signal with short and long incubation times, respectively, upon addition of PtL-Cl, whereas the panels 7c and 7d show the changes in the CD signal upon addition of CuL-Cl.

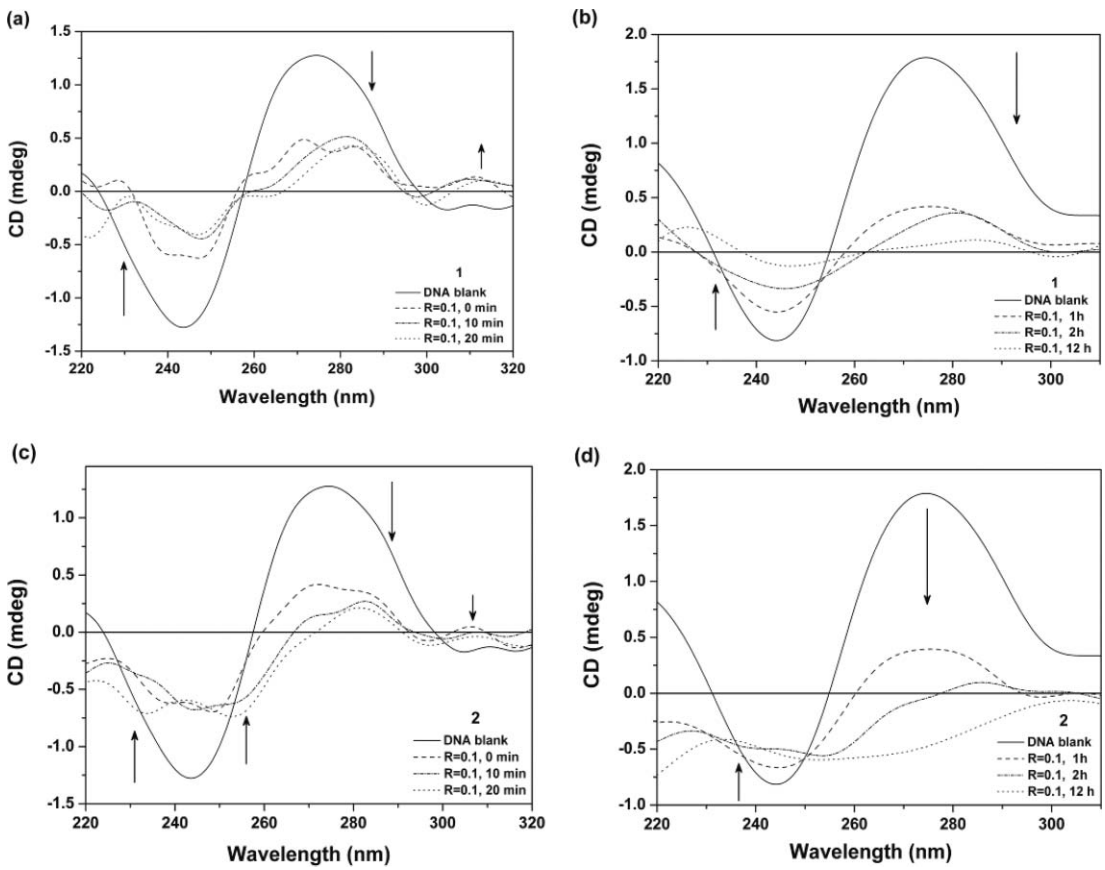

Fig. 7 Time-dependent conformational changes of right-handed DNA upon addition of PtL-Cl and CuL-Cl, in phosphate buffer (10 mM) at pH = 7.2 at 37 °C with R = 0.1. The panels (a) and (c) show the changes in the CD signal for PtL-Cl (1) and CuL-Cl (2), respectively, after a short reaction time. The panels (b) and (d) show the changes in the CD signal after prolonged exposure of CT-DNA to PtL-Cl and CuL-Cl, respectively.

The right handed B-DNA exhibits dramatic changes on its characteristic positive and negative bands at 272 and 248 nm, respectively, on interaction with of PtL-Cl and CuL-Cl [Fig. 7(a-d)]. The changes started immediately after addition of the compounds to the DNA solution and were observed till 12 h after incubation. PtL-Cl induces a decrease in intensity for both the positive (272 nm) and negative bands (248 nm). Also, new negative (at 230 nm) and positive (at 310 nm) bands were observed, respectively, as part of the DNA structural degradation. The decrease in positive band intensity indicates destabilization of base-stacking and the decrease in the negative band intensity points to loss in right-handed helicity.[41] A similar behaviour was observed for CuL-Cl. The changes observed immediately on incubation of PtL-Cl and CuL-Cl reveal the DNA degradation or unwinding due to strong interaction with the compounds. Also the systematic decrease in the intensities of the bands is a proof for a uniform, specific type of interaction for the PtL-Cl and CuL-Cl with DNA, rather than a random mode of interaction. The total loss of the DNA helicity and disruption of the base stacking can be easily correlated to the DNA cleavage activity of PtL-Cl and CuL-Cl.[42] In a recent report[41] the reduction in the intensity of the positive band is reported to originate from interstrand crosslinks to DNA (similar as transplatin). Indeed, the single chloride can be hydrolysed forming a positively charged species that can assist the first electrostatic interaction of the metal compounds with the DNA strand, followed by intercalation of the planar ligand between the base pairs. Therefore, the combined effect of intercalation and coordination is probable for both PtL-Cl and CuL-Cl, to allow an effective DNA interaction and cause oxidative damage.[41,43]

The CD spectral changes in DNA induced by the starting free ligand, Hpyramol is shown in Fig. S3.† The concentrations of DNA used were 50 μM (per base) and 500 μM ligand, with the same R value of 0.1 as in the other samples. There is a slight hyperchromic change in the positive maxima (278 nm) with a blue shift of 2 nm. The reduction in intensity of the negative band and its 1 nm red shift are also well marked. The appearance of the new band at 230 nm is observed for both PtL-Cl and CuL-Cl. In spite of the changes in intensity, the base-stacking and right-handed helicity are retained, revealing that the ligand only interacts, probably through intercalation with DNA, but does not induce DNA cleavage. Thus the CD spectral changes can be directly correlated with the DNA-cleavage properties observed with agarose gel electrophoresis.

The reference compound, cisplatin, is a classical example of a metallodrug which binds to DNA by coordination. The CD spectra in the presence of cisplatin remain mostly unperturbed as a function of time (Fig. S3†). Initially the positive band intensity slightly decreased and 2 nm red shift was observed after 12 h of incubation. The base stacking remained stabilised in time and the helicity of the right-handed B-DNA was found slightly disturbed. The reduced intensity in the negative maximum (248 nm) can be easily explained by the unwinding of the helix/or by DNA kinking, which is caused by intrastrand and interstrand crosslinks. Similar CD spectral changes were observed for all above compounds, when the ϕX174 supercoiled phage DNA was used for measurements instead of calf thymus DNA (data not shown).

Spectro-electrochemical studies

Cyclic voltammetric scans of PtL-Cl at a Pt microdisk electrode were conducted at room temperature in dry deaerated DMF. In the anodic region, the cyclic voltammogram shows an irreversible wave (O1) at $E_{p,a} = +1.28$ V *vs* Ag/AgCl for $v = 100$ mV s^{-1} (Fig. 8a). A well-separated cathodic wave (R1) is observed at $E_{p,c} = +0.25$ V on the reverse scan. The reference compound CuL-Cl exhibits a very similar anodic behaviour ($E_{p,a} = +1.11$ *vs* Ag/AgCl in MeCN), which was explained by axial solvent coordination to oxidised [CuL-Cl]$^+$.[44] The anodic peak is attributed to the oxidation of the phenolate part of the coordinated pyrimol ligand to phenoxyl radical. The largely pyrimol (phenolate) localised oxidation[44] corresponds with the similar oxidation potentials of PtL-Cl and CuL-Cl. The small $E_{p,a}$ shift may have origin in different kinetics of the coupled chemical reaction (solvent coordination) and/or reflects the minor contribution of metal d orbitals into the HOMO. A better insight should be obtained by DFT calculations of PtL-Cl which, however, were considered as out of scope of this work. The phenolate oxidation in PtL-Cl can also be compared with the oxidation of the dehydrogenated Hpyrimol ligand in DMF (Fig. 8b), which is also irreversible and slightly positively shifted to $E_{p,a} = +1.35$ V *vs* Ag/AgCl. In the latter case, however, the coupled chemical reaction might have a different origin (*e.g.*, deprotonation).

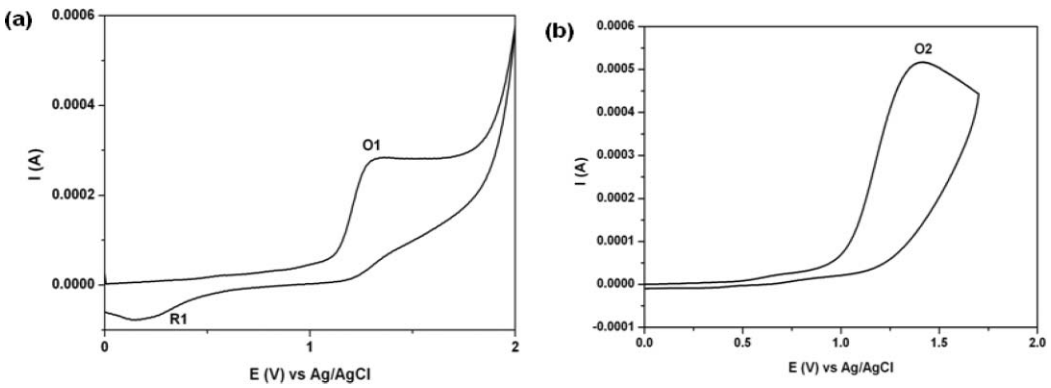

Fig. 8 Cyclic voltammograms of 10^{-3} M PtL-Cl (a) and the free ligand, Hpyrimol (b) in the anodic region. Conditions: freshly polished Pt working electrode (apparent surface area of 0.312 cm^2), $v = 100$ mV s^{-1}, DMF/10^{-1} M Bu_4NPF_6, room temperature.

The UV-Vis spectrum of PtL-Cl in dry DMF shows prominent absorption bands at 620, 425 and 310 nm. These bands are replaced during the oxidation at the O1 electrode potential (+1.28 V *vs* Ag/AgCl) by new absorptions at 260 (sh) and 380 (sh) nm and a poorly resolved absorption between 400–600 nm (Fig. 9). The visible absorption of the oxidised species reflects the presence of the phenoxyl radical ligand (L$^{\bullet}$) derived from pyrimol. The UV-Vis spectrum of short-lived free L$^{\bullet}$ (shoulder at *ca.* 430 nm)[45] is shown in the Supporting Information (Fig. S4†). For oxidised [CuL$^{\bullet}$-Cl]$^{+}$, the corresponding electronic transitions between 400-500 nm were shown by TD-DFT to have a mixed intraligand (L$^{\bullet}$) and charge-transfer (Cu-to-L$^{\bullet}$) character.[44] The involvement of the transition metal centre in the visible electronic excitation may explain the low-energy shift of the absorption to 500-600 nm for [PtL$^{\bullet}$-Cl]$^{+}$ (Fig. 9) compared to CuL-Cl.

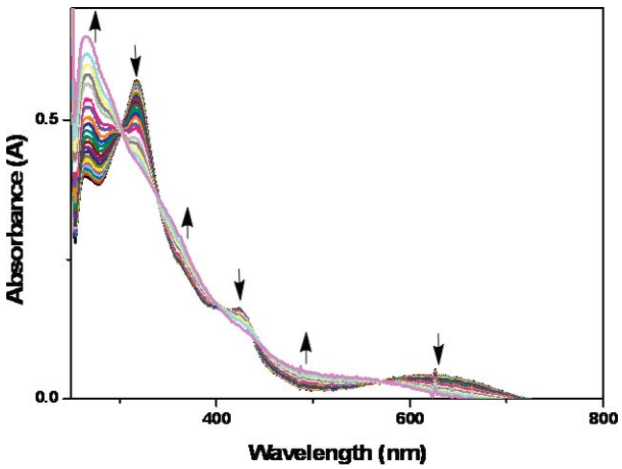

Fig. 9 UV-Vis spectral changes accompanying the rapid oxidation of PtL-Cl at the electrode potential O1 to a phenoxyl radical species in DMF at room temperature, using an OTTLE cell.

Differently from fairly stable [CuL$^{\bullet}$-Cl]$^{+}$ that could be reduced back on the time scale of min to largely recover the neutral parent compound,[44] the oxidised [PtL$^{\bullet}$-Cl]$^{+}$ species is more reactive at room temperature, as concluded from a constant decay of its absorption in the OTTLE cell prior to the reverse reduction at the cathodic wave R1. The apparent difference in the relative stability of the phenoxyl radical complexes may explain the higher (catalytic) activity of CuL-Cl towards the DNA substrate, as described in this work. The species [CuL$^{\bullet}$-Cl]$^{+}$ was shown by cyclic voltammetry to bind reversibly a solvent molecule, probably at the axial position.[44] In strictly square planar [PtL$^{\bullet}$-Cl]$^{+}$ the expected strong *trans* effect labilises the Pt-Cl bond, causing dissociation of the chloride ligand and solvent coordination, being probably coupled to further reactivity. The existence of the solvent-substituted species [Pt(pyrimol)(Sv)]$^{+}$ (Sv = DMF or DMSO) formed during the reaction of PtL-Cl with model DNA bases in these donor solvents, as revealed by ESI-MS (see below), supports strongly this argumentation.

Reactions with DNA model bases

9-Ethylguanine. The reaction between PtL-Cl and 9-EtG, typically in the molar ratios 1:1 and 1:4, was monitored by ^{1}H and ^{195}Pt NMR spectroscopy. 9-EtG was dissolved in DMSO-d_6 and spectra were recorded at physiological temperature (37 °C). Also the time-dependent ESI-MS studies were performed to determine the relative formation rate of the adduct. The reaction mixture showed the presence of unreacted reagents (PtL-Cl and 9-EtG) and very small peaks arising from the mono-adduct independently of the molar excess of the model base. The time-dependent serial spectra (^{1}H NMR) showed only small changes (Fig. 10). However, a new peak in ^{195}Pt NMR at –2405 ppm was clearly observed after 48 h, which can be assigned to a PtN_3O moiety.

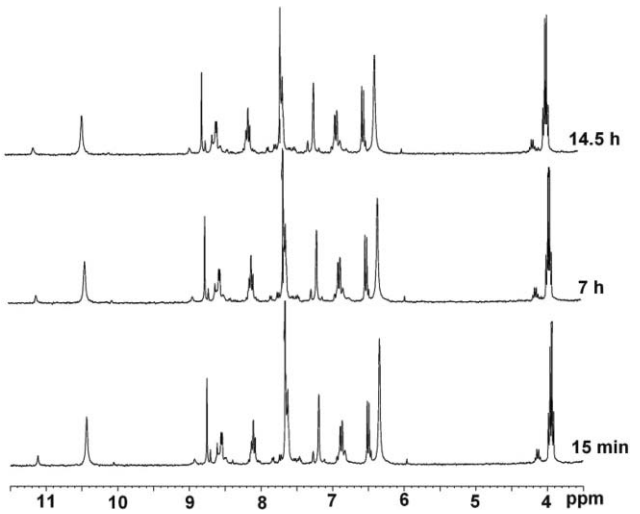

Fig. 10 Stacked ^{1}H NMR spectra of PtL-Cl in presence of 9-EtG (1:1) in DMSO-d_6 at 37 °C.

The ESI-MS also proves the gradual evolution of the adduct, [Pt(pyrimol)(9-EtG)]Cl at m/z = 620.96. In the reaction mixture the species present can be assigned as (a) [Pt(pyrimol)(dmso)]$^{+}$; m/z = 483.91, (b) [Pt(pyrimol)(9-EtG)]$^{+}$; m/z = 585.86; (c) [Pt(pyrimol)(9-EtG)(dmso)]$^{+}$; m/z = 662.79, (d) 9-EtG; m/z = 178.92 and (e) 9-EtG+DMSO; m/z = 253.99. The platinum-containing species show the typical Pt isotopic pattern. The major component of the reaction mixture is the solvated product, [Pt(pyrimol)(dmso)]$^{+}$. The reaction is not immediate, but the appearance of this mono-adduct was observed by ESI-MS (see Fig. S5†) and NMR only after 24 h.

5′-Guanosine monophosphate. PtL-Cl was allowed to react with this model base in different molar ratios (namely 1:1 and 1:4) in a solvent mixture of DMSO-d_6 and D_2O at 37 °C. The changes in NMR and ESI-MS spectra were followed in certain time intervals. The poor solubility of PtL-Cl in aqueous solvent and no solubility of GMP in organic solvent, limits the use of PtL-Cl at high concentrations. The clear progress of ^{1}H NMR changes is shown in stacked spectra (Fig. 11). The ^{195}Pt NMR revealed a new signal at –2820 ppm after 24 h (N_2OS coordination environment around Pt)[39,40] quite changed from the peak from the starting compound PtL-Cl at –2319 ppm (in DMSO-d_6+D_2O). Results of a time-dependent ESI-MS study performed in DMF (shown in Fig. S6) document the presence of a mixture of adducts assigned (a) [Pt(pyrimol)(dmf)]$^{+}$ (*i.e.*, solvolysis in presence of DMF); m/z = 479.87, (b) [Pt(pyrimol)]$^{+}$ +3 CH_3OH (eluting solvent); m/z = 537.86 (major), (c) [Pt(pyrimol)]$^{+}$ + 2 DMF; m/z = 552.82, (d) [Pt(pyrimol)(GMP)]; m/z = 842.97, (e) [Pt(pyrimol)(GMP)] + DMF; m/z = 921.71. Therefore the mono-substituted adduct can

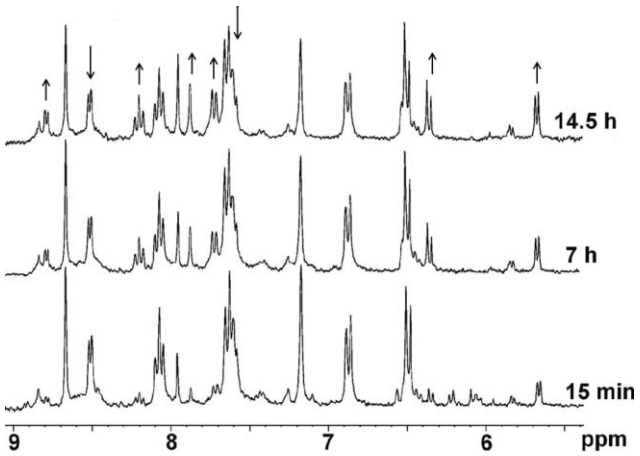

Fig. 11 Time-dependent changes in ^{1}H NMR spectra of PtL-Cl upon addition of 5′-GMP in DMSO-d_6 + D_2O at 37 °C. The arrows show gradual changes (rise of a new peak [up] or decrease of a peak [down] with time).

be identified, but the solvent-coordinated species is the major one and is not easily substituted by model base.

Interaction with d(GTCGAC)$_2$

The interaction of PtL-Cl with the self complementary oligonucleotide d(GTCGAC)$_2$[46] was carried out at different temperatures ranging from 4-47 °C to obtain a slow or fast proton exchange rather than an intermediate exchange. ^{1}H NMR spectra were recorded in 90% H_2O and 10% D_2O to follow any changes in the amine/imine protons of the oligonucleotide. The variable temperature 1-D, ^{1}H NMR experiments show that at 17 °C (Fig. S7) and 27 °C (Fig. S8)† fast exchanges were observed and the Tables 4 and 5 clearly describes the proton shifts (in ppm) for the PtL-Cl (free) and after interacting with the oligonucleotide at 17 °C and 27 °C. The used numbering of the protons is depicted in the insert with the ^{1}H NMR spectra in Fig. S8.† The assignments were based on 2D DQF-COSY, through bond interactions at 27 °C; they were done for the pure PtL-Cl compound and for PtL-Cl after interaction with the oligonucleotide at 27 °C (Figs. S9 and S10).† In general, the bound compound shows large shifts of the ligand proton signals, especially in the phenolate part (3H and 4H) compared to the less affected methylene protons (signal 9H) and medium shifted pyridine ring proton signals 11H to 14H, (Figs. S8 and S11).† The totally decayed appearance of signal

Table 4 ^{1}H NMR signals (δ in ppm) of PtL-Cl before and after the interaction with oligonucleotide

PtL-Cl–protons	No oligonucleotide	In the presence of d(GTCGAC)$_2$ at 27 °C	In the presence of d(GTCGAC)$_2$ at 17 °C
3 (d)	6.89	8.22	8.23
4 (d)	6.50	7.72	7.71
6 (s)	8.77	7.58	7.60
9 (s)	7.20	7.34	7.38
11 (d)	7.64	7.96	7.90
12 (t)	8.12	8.17	8.16
13 (t)	7.64	7.43	7.41
14 (d)	8.55	7.98	7.97

Table 5 ^{1}H NMR signals (δ in ppm) of oligonucleotide before and after interaction with PtL-Cl

d(GTCGAC)$_2$ - protons	Free (no PtL-Cl)	With PtL-Cl at 27 °C	With PtL-Cl at 17 °C
8H of G1	7.946	8.016	8.031
8H of G4	7.458	7.982	8.031
8H of A5	7.921	7.982	8.014
2H of A5	8.132	8.053	8.052
5H of C3	5.589	6.523	6.520
5H of C6	5.262	6.940	6.963
6H of C3	7.446	6.725	6.712
6H of C6	7.257	7.114	7.124
6H of T2	7.496	7.535	7.538
2′	1.8–3.0	—	—
4′;5′	3.7–4.5	—	—
3′	4.4–5.2	—	—
1′	5.3–6.3	—	—

11 and the approximately 1.5 ppm downfield shifts observed for the signals 3H and 4H, clearly reveal the intercalating mode of interaction for the PtL-Cl through the pyrimol ligand between the nucleobases. Further, the shifts of the oligonucleotide proton signals can be observed for all the base protons, but the highest is with cytosine (C3H5, C3H6) and guanine (G4H8) protons in the central position of the oligonucleotide. Again, the proton assignment was achieved by comparing the 2-D DQF-COSY spectrum of the free oligonucleotide and the 2-D DQF-COSY spectrum of d(GTCGAC)$_2$ interacting with PtL-Cl at 27 °C. The sugar protons could not be followed individually, due to broad and merged signals after interaction with the Pt compound. The same kind of broadened signals were observed for the amino/imino protons, immediately after interacting with PtL-Cl, making it difficult to follow the signal in time, also in 2-D experiments. Based on the assignments, the NOESY spectrum at 27 °C was also analysed to detect any through space interactions between the oligonucleotide and PtL-Cl (within 4 Å, Fig. S12).† The cross peaks observed between (i) the ligand proton 9 to C3H5/C6H5; (ii) 6 to the 1′ sugar protons and (iii) 13 the 3′ sugar protons, are important to reveal that the compound tends to interact in the minor groove of the oligonucleotide at the fast exchange rate.[47] That is from the C3 to the C6 region of d(GTCGAC)$_2$, which is also obvious from the proton shifts associated with the corresponding bases. For the small molecules like Cu(phen)$^{2+}$ the minor groove binding is suggested for a compact and closer DNA interaction. Thus the simple, planar PtL-Cl could also be expected to interact initially with DNA in the minor groove. The unassigned peaks observed in the 1-D spectra (data not shown) after 8 h of interaction can be assumed as arising from the cleaved DNA (sugars/bases), which again supports a non-specific DNA cleavage event occurring on interaction with PtL-Cl.

Conclusions

A novel platinum compound was synthesised and characterised in detail by NMR and X-ray analysis. The Pt(II) ion is in a square-planar coordination environment with the ligand having a tripodal (N,N,O) chelating motif. The ligand precursor Hpyramol was found to dehydrogenate and form the pyrimol anion that binds firmly to Pt(II). This compound induces single-strand scission of supercoiled DNA, just like the previously reported[26]

analogue CuL-Cl, *albeit* in stoichiometric concentrations rather than catalytic amounts. Both compounds show high to modest *in vitro* cytotoxic properties against various cancer cell lines. The cancer cell-growth inhibition ability appears to be strongly time-dependent and selective towards some cell lines. The cytotoxic activity induced by CuL-Cl may be explained by catalytic DNA cleavage, which results in irreparable damage, different cellular processing and the bioavailability inside the cells. The comparatively low activity of PtL-Cl indicates reversible DNA damage, facile repair mechanism, higher stability of solvated intermediate and non-availability of the active species in intracellular medium. To correlate the DNA cleavage properties, *in vitro* cytotoxicity and the DNA structural changes, several techniques were used to provide mechanistic insights.

The spectro-electrochemical studies of PtL-Cl in comparison with CuL-Cl and free Hpyrimol provide supportive evidence for the formation of a phenoxyl radical and its likely involvement in oxidative DNA-cleavage. The structural changes of the DNA were followed by circular dichroism and gel mobility studies and the observed DNA degradation by PtL-Cl was further analysed in detail by high-resolution gel electrophoresis. These experiments not only indicated extensive DNA degradation, but also demonstrated that PtL-Cl cleaves nucleotides simultaneously or sequentially at multiple positions. The reactions of PtL-Cl with DNA model bases (9-ethylguanine and 5′-GMP; 1:1) at physiological temperature exhibit the slow formation of mono-adducts with chloride substitution *via* solvolysis. Our studies also highlighted that PtL-Cl primarily interacts with the minor groove of the DNA, in contrast to cisplatin which preferentially binds to the major groove.

The title compound PtL-Cl induces significant damage to isolated DNA under experimental *in vitro* conditions of biophysical studies; however, DNA damage inside the cancer cells might be easily reparable. Being a monofunctional compound, PtL-Cl induces comparatively lower cytotoxicity than cisplatin in a panel of cell lines. The mono-adduct formed on the DNA helix in the minor groove by small PtL-Cl, is unable to widen the minor groove. As a result the typical 'kink' of cisplatin interaction is not induced and the DNA degradation is eventually repaired by the cell machinery.

Thus the DNA-targeting monofunctional platinum compound possessing dual intercalation-coordination property in fact acts as minor-groove binder and simultaneously overcomes the resistance. The present work, including all the mechanistic studies, strongly suggests that a controlled modification, could lead to new, potential antitumour compounds that can survive the repair mechanism and induce facile apoptosis.

Acknowledgements

We are grateful to Prof. Dr. Jaap Brouwer for his support (in-house cytotoxicity and uptake) and to TEVA-Pharmachemie, Haarlem (The Netherlands) for conducting the cell viability assays. Johnson-Matthey (Reading, UK) is gratefully thanked for their generous donation of K_2PtCl_4. The work described here was financially supported (M. L., A. L. S.) by the Council for Chemical Sciences of the Netherlands Organization for Scientific Research (CW-NWO).

References

1 L. Kelland, *Nat. Rev. Cancer*, 2007, **7**, 573–584.
2 B. Lippert, *Cisplatin, Chemistry and Biochemistry of a Leading Anticancer Drug*, Wiley-VCH, Weinheim, 1999.
3 L. Kelland, *Expert Opin. Invest. Drugs*, 2007, **16**, 1009–1021.
4 E. R. Jamieson and S. J. Lippard, *Chem. Rev.*, 1999, **99**, 2467–2498.
5 J. Reedijk, *Chem. Rev.*, 1999, **99**, 2499–2510.
6 J. Reedijk, *Curr. Opin. Chem. Biol.*, 1999, **3**, 236–240.
7 Y. W. Jung and S. J. Lippard, *Chem. Rev.*, 2007, **107**, 1387–1407.
8 D. Wang and S. J. Lippard, *Nat. Rev. Drug Discovery*, 2005, **4**, 307–320.
9 J. Reedijk, *Proc. Natl. Acad. Sci. U. S. A.*, 2003, **100**, 3611–3616.
10 J. Reedijk, *Platinum Met. Rev.*, 2008, **52**, 2–11.
11 M. D. Hall, M. Okabe, D. W. Shen, X. J. Liang and M. M. Gottesman, *Annu. Rev. Pharmacol. Toxicol.*, 2008, **48**, 495–535.
12 X. Gao, X. Wang, J. Ding, L. Lin, Y. Li and Z. Guo, *Inorg. Chem. Commun.*, 2006, **9**, 722–726.
13 F. Huq, J. Qing Yu, H. Daghriri and P. Beale, *J. Inorg. Biochem.*, 2004, **98**, 1261–1270.
14 H. Tayyem, F. Huq, J. Q. Yu, P. Beale and K. Fisher, *ChemMedChem*, 2008, **3**, 145–151.
15 A. D. Richards and A. Rodger, *Chem. Soc. Rev.*, 2007, **36**, 471–483.
16 S. Roy, K. D. Hagen, P. U. Maheswari, M. Lutz, A. L. Spek, J. Reedijk and G. P. van Wezel, *ChemMedChem*, 2008, **3**, 1427–1434.
17 L. S. Hollis, W. I. Sundquist, J. N. Burstyn, W. J. Heiger-Bernays, S. F. Bellon, K. J. Ahmed, A. R. Amundsen, E. W. Stern and S. J. Lippard, *Cancer Res.*, 1991, **51**, 1866–1875.
18 R. Guddneppanavar, G. Saluta, G. L. Kucera and U. Bierbach, *J. Med. Chem.*, 2006, **49**, 3204–3214.
19 K. S. Lovejoy, R. C. Todd, S. Z. Zhang, M. S. McCormick, J. A. D'Aquino, J. T. Reardon, A. Sancar, K. M. Giacomini and S. J. Lippard, *Proc. Natl. Acad. Sci. U. S. A.*, 2008, **105**, 8902–8907.
20 V. Bursova, J. Kasparkova, C. Hofr and V. Brabec, *Biophys. J.*, 2005, **88**, 1207–1214.
21 Y. Ma, C. S. Day and U. Bierbach, *J. Inorg. Biochem.*, 2005, **99**, 2013–2023.
22 A. T. M. Marcelis, C. Erkelens and J. Reedijk, *Inorg. Chim. Acta*, 1984, **91**, 129.
23 P. de Hoog, M. J. Louwerse, P. Gamez, M. Pitié, E. J. Baerends, B. Meunier and J. Reedijk, *Eur. J. Inorg. Chem.*, 2008, 612–619.
24 L. D. Pachon, A. Golobic, B. Kozlevcar, P. Gamez, H. Kooijman, A. L. Spek and J. Reedijk, *Inorg. Chim. Acta*, 2004, **357**, 3697–3702.
25 P. U. Maheswari, S. Barends, S. Ozalp-Yaman, P. de Hoog, H. Casellas, S. J. Teat, C. Massera, M. Lutz, A. L. Spek, G. P. van Wezel, P. Gamez and J. Reedijk, *Chem.–Eur. J.*, 2007, **13**, 5213–5222.
26 P. U. Maheswari, S. Roy, H. den Dulk, S. Barends, G. van Wezel, B. Kozlevcar, P. Gamez and J. Reedijk, *J. Am. Chem. Soc.*, 2006, **128**, 710–711.
27 A. J. M. Duisenberg, L. M. J. Kroon-Batenburg and A. M. M. Schreurs, *J. Appl. Crystallogr.*, 2003, **36**, 220–229.
28 G. M. Sheldrick, *SADABS: Area-Detector Absorption Correction*, (1999) Universität Göttingen, Germany.
29 P. T. Beurskens, G. Admiraal, G. Beurskens, W. P. Bosman, S. Garcia-Granda, R. O. Gould, J. M. M. Smits, C. Smykalla, *The DIRDIF99 program system, Technical Report of the Crystallography Laboratory*, University of Nijmegen, Nijmegen, The Netherlands, 1999.
30 G. M. Sheldrick, *Acta Crystallogr., Sect. A: Found. Crystallogr.*, 2007, **64**, 112–122.
31 A. L. Spek, *J. Appl. Crystallogr.*, 2003, **36**, 7–13.
32 T. Mosmann, *J. Immunol. Methods*, 1983, **65**, 55–63.
33 Y. P. Keepers, P. E. Pizao, G. J. Peters, J. Vanarkotte, B. Winograd and H. M. Pinedo, *European Journal of Cancer and Clinical Oncology*, 1991, **27**, 897–900.
34 M. R. Boyd, in *Cancer: Principles and Practice of Oncology Update*, ed. H. De Vita V. T. Jr., S. and S. A. Rosenberg, Lippincott Philadelphia, 1989, vol. 3, pp. 1-12.
35 S. Rigali, F. Titgemeyer, S. Barends, S. Mulder, A. W. Thomae, D. A. Hopwood and G. P. van Wezel, *EMBO Rep.*, 2008, **9**, 670–675.
36 M. Krejčik, M. Daněk and F. Hartl, *J. Electroanal. Chem.*, 1991, **317**, 179–187.
37 M. A. Weiss, J. L. Eliason and D. J. States, *Proc. Natl. Acad. Sci. U. S. A.*, 1984, **81**, 6019–6023.
38 M. Piotto, V. Saudek and V. Sklenář, *J. Biomol. NMR*, 1992, **2**, 661–665.
39 J. R. L. Priqueler, I. S. Butler and F. D. Rochon, *Appl. Spectrosc. Rev.*, 2006, **41**, 185–226.

40 B. M. Still, P. G. A. Kumar, J. R. Aldrich-Wright and W. S. Price, *Chem. Soc. Rev.*, 2007, **36**, 665–686.
41 J. Kašpárková, M. Vojtíšková, G. Natile and V. Brabec, *Chem.–Eur. J.*, 2008, **14**, 1330–1341.
42 V. Brabec and J. Kašpárková, *Drug Resist. Updates*, 2005, **8**, 131–146.
43 V. Brabec, V. Boudný and Z. Balcarová, *Biochemistry*, 1994, **33**, 1316–1322.
44 P. U. Maheswari, *et al.*, *Eur. J. Inorg. Chem.*, 2009, to be submitted.
45 V. T. Kasumov, H. Turkmen, I. Ucar, A. Bulut and N. Yayli, *Spectrochim. Acta, Part A*, 2008, **70**, 60–68.
46 P. U. Maheswari, V. Rajendiran, H. Stoeckli-Evans and M. Palaniandavar, *Inorg. Chem.*, 2006, **45**, 37–50.
47 J. P. Rehmann and J. K. Barton, *Biochemistry*, 1990, **29**, 1710–1717.